ISSN 1068-3666, Journal of Friction and Wear, 2022, Vol. 43, No. 2, pp. 128–134. © Allerton Press, Inc., 2022.
Russian Text © The Author(s), 2022, published in Trenie i Iznos, 2022, Vol. 43, No. 2, pp. 192–201.

Influence of Flattening in the Zone of Welded Joints of Railroad Track on Contact Interaction in the Wheel–Rail System

A. R. Meshcheryakova[a, b, *] and I. Yu. Tsukanov[a, b]

[a] *Institute for Problems in Mechanics, Russian Academy of Sciences, Moscow, 119526 Russia*
[b] *Sirius University of Science and Technology, Sochi, 354340 Russia*
**e-mail: mif-almira@yandex.ru*

Received October 14, 2021; revised April 15, 2022; accepted April 18, 2022

Abstract—The wheel–rail interaction during rolling along a straight railroad track section with and without the rail flattening effect is modeled. Rail flattening is used to describe a defect that occurs in the area of a welded rail joint. The model takes into account an increase in the load during dynamic impactless interaction in the region of welded joints, change in the configuration of the contact region, and existence of stick and slip subregions during rolling. The contact characteristics and stress states of the rail are compared for different relative longitudinal slip and in the presence and absence of track flattening of two characteristic sizes. An analysis of internal stresses shows that an increase in the relative longitudinal slip leads to an increase in the maximal tangential stresses near the surface. The results of analyzing contact pressures and tangential stresses show that, with an increase in the flattening depth, the depth wise distribution of maximal tangential stresses becomes more uniform.

Keywords: wheel, rail, contact stresses, welded joints, flattening, rolling, stick and slip subregions
DOI: 10.3103/S1068366622020088

INTRODUCTION

An important role in predicting the durability of rolling stock wheel pairs is played by the calculation of the accumulation of contact-fatigue failures [1]. The passing of wheel pairs over railroad irregularities increases the loads and changes the conditions of the wheel-rail contact, which encourages the cyclic change in the stress state in the contact zone and accumulation of fatigue damage [2].

Welded rail bond defects are generated over time during the passing of rolling stock. Such defects are most often shaped as saddles [3] and are caused by local rail head crushing during exposure to contact stresses due to the existence of low-hardness sections in the welded joint area [3].

As shown by analyzing dynamic loads and change in the longitudinal rail profile in the welded joint flattening area depending on passed tonnage [2], longitudinal saddling length L changes much slower with an increase in passed tonnage in comparison with saddling depth h_0. Typical saddling dimensions are h_0 = 1–3 mm and L = 200–250 mm. That said, according to [2], at saddling depth h_0 = 1.6 mm the vertical load increased by 12.3%.

The dynamic load during the passing of a wheel pair over railroad irregularities is computed by both, modeling in commercial and specialized software suites [4, 5] and using approximate analytical models [6].

The modeling of the accumulation of contact-fatigue damage includes the computation of the stress state in the wheel–rail contact; this state is defined by distributions of contact pressures and tangential stresses. For these purposes, the FASTSIM algorithm [7] and its upgraded models are broadly applied. The numerical solution of the elastic body rolling problem in the spatial formulation, considering slip and spinning, is shown in [8, 9]. This solution is necessary for calculating the stress state.

The generation of contact-fatigue failures of rails and freight car wheels is modeled in [1, 10, 11]. The maximal tangential stresses, depending on external load and configuration of the wheel–rail contact region, are used as one of the damage criteria.

Objective—To simulate the wheel–rail interaction to compare the contact characteristics and stress state without track flattening and considering the weld joint flattening defect.

DETERMINATION OF CONTACT CHARACTERISTICS IN THE WHEEL–RAIL SYSTEM

Calculation in the Absence of Track Irregularities

Let us consider the contact of a wheel and a rail during the motion along a straight track section without irregularities as a contact of elastic bodies with

equal elastic material constants, that is, Young's modulus E and Poisson's ratio ν (the respective E and ν of steel are 210 GPa and 0.3).

The contact pressure distribution is calculated using the Hertz solution of the two-bodies contact problem [12]:

$$p_1 = p_{0_1}\left(1-\left(\frac{x}{a_1}\right)^2-\left(\frac{y}{b_1}\right)^2\right)^{\frac{1}{2}}, \quad p_{0_1}=\frac{3}{2}\frac{P}{\pi a_1 b_1}, \qquad (1)$$

$$a_1 = m\left(\frac{3}{4}\frac{P(k_1+k_2)}{(A+B)}\right)^{\frac{1}{3}}, \quad b_1 = n\left(\frac{3}{4}\frac{P(k_1+k_2)}{(A+B)}\right)^{\frac{1}{3}}, \qquad (2)$$

where a_1 and b_1 are the semiaxes of the elliptical contact region, p_{0_1} is the highest contact pressure, P is the full normal wheel load, $k_i = (1-\nu_i^2)/E_i$, $i = 1,2$; $i = 1$ corresponds to the wheel, and $i = 2$ corresponds to the rail. Coefficients A and B are determined as

$$A+B = \frac{1}{2}\left(\frac{1}{R_1}+\frac{1}{R_1'}+\frac{1}{R_2}+\frac{1}{R_2'}\right), \qquad (3)$$

$$B-A = \frac{1}{2}\left[\left(\frac{1}{R_1}-\frac{1}{R_1'}\right)^2+\left(\frac{1}{R_2}+\frac{1}{R_2'}\right)^2+2\left(\frac{1}{R_1}-\frac{1}{R_1'}\right)\left(\frac{1}{R_2}-\frac{1}{R_2'}\right)\cos 2\psi\right]^{\frac{1}{2}}, \qquad (4)$$

where R_1 and R_1' are the main wheel curvature radii, R_2 and R_2' are the main rail curvature radii, and ψ is the angle between the normal planes with curvature radii R_1 and R_2.

Calculation in Case of a Saddling Defect in the Welded Joint Region

The longitudinal profile of a flattening in the welded rail bond region is described by the following dependence corresponding to an irregularity without sharp edges [2]:

$$h(x) = -h_0\left(\sin\left(\frac{\pi x}{L}\right)\right)^2, \qquad (5)$$

where h_0 and L are the saddling depth and length, respectively.

A wheel passes over a rail with a saddling defect at longitudinal speed V in two possible dynamic modes, that is, impact and impactless. In the impact mode the wheel hits the defect edge at a certain angle usually determined by experiments [13]. In the impactless mode the wheel rolls over the saddle (Fig. 1). Considering the small h_0/L ratio typical of measured saddles

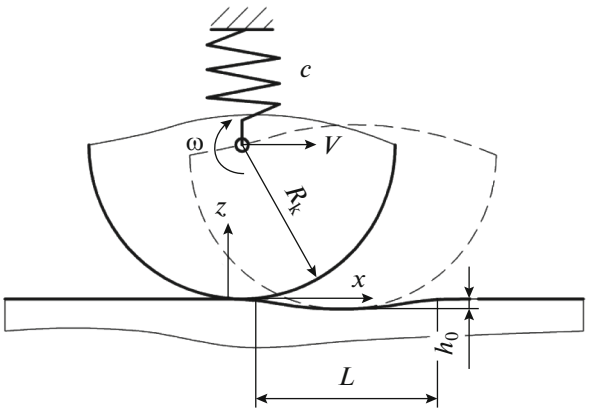

Fig. 1. Scheme of the wheel–rail interaction during the passage of a defect shaped as a saddle.

[2], let us consider that the wheel–rail interaction in the saddle zone is impactless.

To calculate the additional dynamic component of vertical load, let us consider the equations of the wheel motion at the interaction with the rail in the saddling region [13]. If we ignore the rail mass, dampening, and contact stiffness smaller than the vertical stiffnesses of the wheel suspension and the rail as elements of the elastic system, the equation of the relative motion of a sprung wheel is written as

$$x = Vt, \quad m\ddot{z} + cz = -m\ddot{h}, \qquad (6)$$

where t is the time; c is the spring stiffness in the equivalent wheel–rail system; m is the unsprung parts mass; and (.) is for the time derivative. The equivalent spring stiffness can be tentatively calculated proceeding from static wheel load P and static wheel deflection δ: $c = P/\delta$. The value of δ is regulated depending on the type of railroad car and truck model [13].

The equation made up by inserting the first equation of system (9) in (8) and differentiation is

$$m\ddot{z} + cz = \frac{2\pi^2 m h_0 V^2}{L^2}\cos\frac{2\pi V t}{L}. \qquad (7)$$

Equation (10) is the induced oscillation equation solved at $z(0) = 0$ and $\dot{z}(0) = 0$ as

$$z = \frac{1}{mp}\int_0^t\left(\frac{2\pi^2 m h_0 V^2}{L^2}\cos\frac{2\pi V\tau}{L}\right)\sin p(t-\tau)d\tau, \qquad (8)$$

where $p = \sqrt{c/m}$. The equation made up by integrating (11) and using (9) is

$$z = \frac{2\pi^2 h_0 V^2\left(\cos\frac{px}{V}-\cos\frac{2\pi x}{L}\right)}{4\pi^2 V^2 - p^2 L^2}. \qquad (9)$$

At $V > 10$ kph maximal additional equivalent spring deformation $z_{\max}$ due to saddling is achieved at $x =$

$L/2$. The approximate equation for estimating z_{max} at small values of the $pL/2V$ argument is calculated using the expansion of the cosine function in the Taylor series and leaving only the constant and the square term, that is

$$z_{max} \approx \frac{h_0\left(\chi^2 - \frac{\pi^2}{4}\right)}{\chi^2 - 1}, \quad (10)$$

where $\chi = 2\pi V/pL$. At large values of χ, $z_{max} \approx h_0$, that is, the maximal spring deformation is determined only by the saddling depth.

The load dynamic factor is $\eta = 1 + P_{add}/P$, where P_{add} is the additional dynamic vertical wheel load that is determined at a first approximation depending on the saddling depth and the stiffness of the wheel–rail system as

$$\eta = 1 + \frac{cz_{max}}{P} \approx 1 + \frac{z_{max}}{\delta}. \quad (11)$$

In the saddle center region ($x = L/2$) the wheel–rail contact configuration at a first approximation corresponds to the interaction of two cylindrical bodies with equal elastic constants and different curvature radii. The contact pressure is calculated using the Hertz solution for plane strain [12]:

$$p_2(x,y) = p_{0_2}\left(1 - \left(\frac{x}{a_2}\right)^2\right)^{\frac{1}{2}}, \quad p_{0_2} = \left(\frac{\eta PE^*}{2\pi b_2 R}\right)^{\frac{1}{2}}, \quad (12)$$

$$\frac{1}{R} = \frac{1}{R_1} - \frac{1}{R_c}, \quad \frac{1}{E^*} = \frac{1-\nu_1^2}{E_1} + \frac{1-\nu_2^2}{E_2}, \quad (13)$$

where a_2 is the half-width of the contact region in the direction of the x-axis, p_{0_2} is the highest contact pressure, and $R_c \approx L^2/(2\pi^2 h_0)$ is the curvature radius of the saddle surface in its center. Since a rail irregularity is generated by rail head crushing, its sharp edges are smoothed, and the edge effects of contact stress distribution can be neglected.

The problem of calculating tangential contact stresses is solved by the variational method in which the composite function is minimized that is built, considering the boundary conditions for stresses and displacements in the contact interaction region [8]:

$$F[\tau, s(\tau)] = \int_\Omega (\mu p(x,y)|s(x,y)| - \tau(x,y)s(x,y))\,dxdy. \quad (14)$$

In this case, the existence of stick and slip subregions in the contact region is considered. At stationary rolling slip velocity $s(x, y)$ of the rolling body relative to the base is determined as

$$s(x,y) = v(x,y) - V\left(\frac{\partial u_1(x,y)}{\partial x} - \frac{\partial u_2(x,y)}{\partial x}\right), \quad (15)$$

$$v(x,y) = V\Delta_x + \frac{\omega}{2R_1}\left(x^2 + y^2\right), \quad (16)$$

where $u_{1,2}(x,y)$ are the tangent functions of the wheel motion and the rail, respectively, ω and V are the angular and linear wheel rolling velocities, Δ_x is the tentative longitudinal slip calculated as

$$\Delta_x = \frac{V - \omega R_1}{V}, \quad (17)$$

R_1 is the wheel surface curvature radius.

At each point of the rail modeled by an elastic half-space, the internal stress tensor components are calculated by the superposition principle on the basis of Boussinesq and Cerutti solutions [12]. The maximal tangential stresses are determined by the formula from [14] as

$$\tau_{max}(x,y,z) = \frac{1}{2}(\sigma_1(x,y,z) - \sigma_3(x,y,z)), \quad (18)$$

where $\sigma_i(x,y,z)$; $i = 1,2,3$ are the main stresses in the point with coordinates (x,y,z), determined according to the characteristic equation:

$$\begin{vmatrix} \sigma_x - \sigma & \tau_{xy} & \tau_{xz} \\ \tau_{xy} & \sigma_y - \sigma & \tau_{zy} \\ \tau_{xz} & \tau_{zy} & \sigma_z - \sigma \end{vmatrix} = 0, \quad (19)$$

whereby the condition fulfilled in each point of the half-space is

$$\sigma_1(x,y,z) > \sigma_2(x,y,z) > \sigma_3(x,y,z). \quad (20)$$

CALCULATION RESULTS AND ANALYSIS

The geometric parameters accepted as constant in calculating the contact pressure distribution are $\psi = 90°$, $R_1 = 450$ mm, $R_1' = \infty$, $R_2 = \infty$, and $R_2' = 500$ mm. Wheel load P was accepted equal to 122500 N and corresponded to a railroad car weight of 50 t. In this case, at $E_1 = E_2 = 210$ GPa and $\nu = 0.3$, the contact region has the following parameters: $a = 7.5$ mm, $b = 7$ mm, $p_0 = 1120$ MPa, and $g = \sqrt{a/b} \approx 1.04$.

The irregularity length is determined mainly by the initial condition of the rail material and by the parameters of welding and thermal processing. In this study, it is accepted that the saddling length is 250 mm. The irregularity depth depends not only on the initial condition of the rail but also on its loading modes. This depth changes more significantly than the saddling length [2]. Let us consider that during wheel rolling along the rail in the course of plastic deformation the

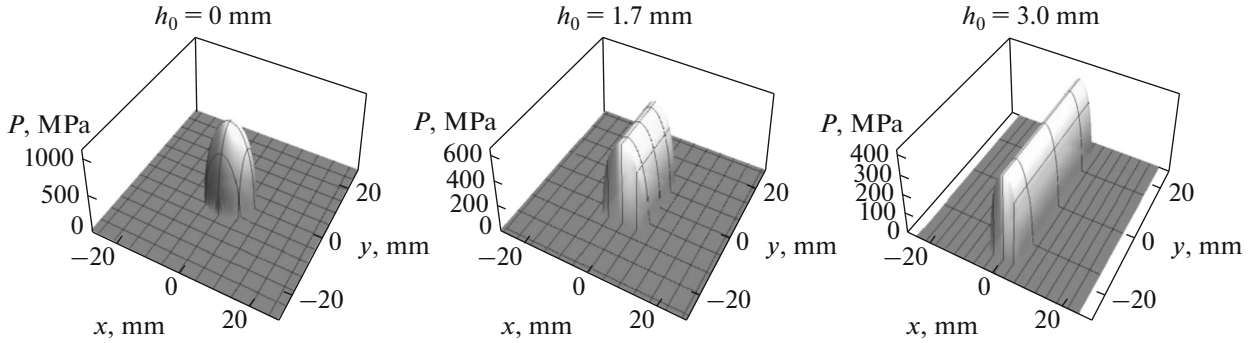

Fig. 2. Distribution of contact pressure at $P = 122.5$ kN.

middle part of the rail head is crushed until it borders with the side planes. Considering the rail head geometry [1], let us consider irregularities with depths $h_0 =$ 1.7 and 3 mm.

The calculations were made at train motion speed $V = 70$ kph and static wheel deflection $\delta = 20$ mm [13]. Dependences (10) and (11) allow determining that at $h_0 = 1.7$ mm and 3 mm load dynamic factor $\eta = 1.085$ and 1.15.

If we proceed from rail head geometry [1], the respective half-widths of the contact region perpendicular to the rolling direction are $b_2 = 10$ and 24.5 mm at $h_0 = 1.7$ and 3 mm. Considering dependence (5), $R_c = 1863$ mm, $P_{add} = 132913$ N, $a_2 = 6.6$ mm, $p_{0_2} =$ 641 MPa, and for the irregularity with $h_0 = 1.7$ mm, $L =$ 250 mm, and = 1055 mm, $P_{add} = 140875$ N, $a_2 =$ 5 mm, $p_{0_2} = 367$ MPa, and for the irregularity with $h_0 = 3$ mm and $L = 250$ mm.

The contact pressure distribution at load $P =$ 122.5 kN on the axis of a 25 t railroad car and at various saddling depths is shown in Fig. 2.

In case of irregularity the maximal contact pressure decreases with an increase in the saddling depth while the contact area increases in which case the change in the contact area width in the rolling direction is insignificant.

The tangential stress distribution for a constant longitudinal slip and contact regions corresponding to the contact pressure distribution (see Fig. 2) is shown in Fig. 3.

With an increase in the saddling depth, the tangential stresses decrease; that said, at $y = 0$ the slippage subregion in the contact region cross-section shrinks.

The influence of relative longitudinal slip on the distribution of tangential stresses for various contact region configurations is illustrated in Fig. 4.

During rolling along a straight section with a twofold increase in longitudinal slip, the slip subregion in the cross section at $y = 0$ increases by 90%. During rolling in the central part of the saddle of 3 mm in depth the subregion increases by 80%.

The dependences of maximal tangential stresses on the z coordinate in the elastic half-space for various longitudinal slip during rolling along a straight track section (solid lines) and at flattenings with $h_0 =$ 1.7 mm (dashes) and $h_0 = 3$ mm (dot-and-dash lines) are shown in Fig. 5.

The isocurves of the maximal tangential stresses in the contact region cross section at $y = 0$ during wheel

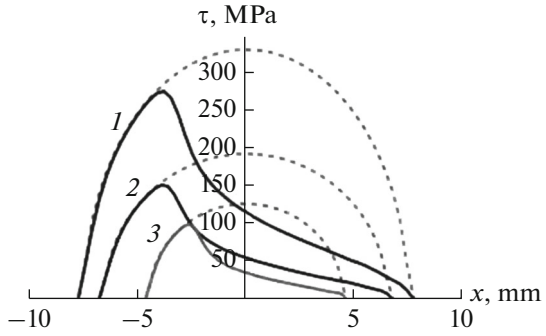

Fig. 3. Distribution of tangential stresses at $\Delta_x = 0.001$ and rail without saddling (*1*) and at rail saddling depth $h_0 =$ 1.7 mm (*2*), $h_0 = 3$ mm (*3*).

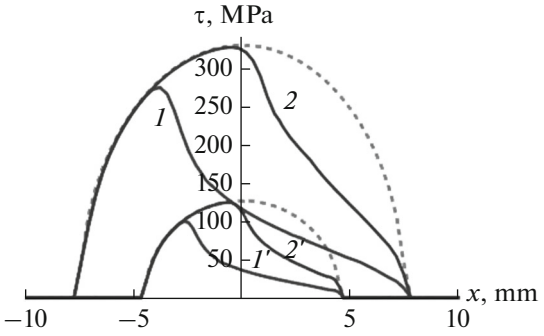

Fig. 4. Distribution of tangential stresses at relative slip $\Delta_x = 0.001$ (*1*, *1′*), $\Delta_x = 0.002$ (*2*, *2′*) without saddling (*1*, *2*) and at rail saddling depth $h_0 = 3$ mm (*1′*, *2′*).

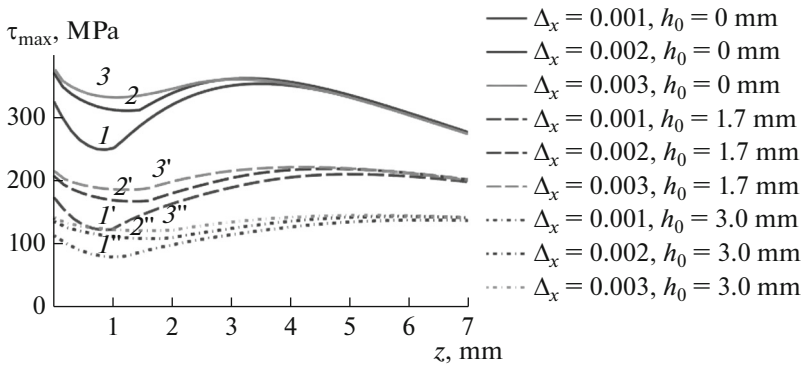

Fig. 5. Dependence of the maximal tangential stresses on the distance to the surface at $\Delta_x = 0.001$ (*1*, *1*', *1*''), $\Delta_x = 0.002$ (*2*, *2*', *2*''), $\Delta_x = 0.003$ (*3*, *3*', *3*''), for rails without irregularity (*1*–*3*), and at rail irregularity depth $h_0 = 1.7$ mm (*1*'–*3*'), $h_0 = 3$ mm (*1*''–*3*'').

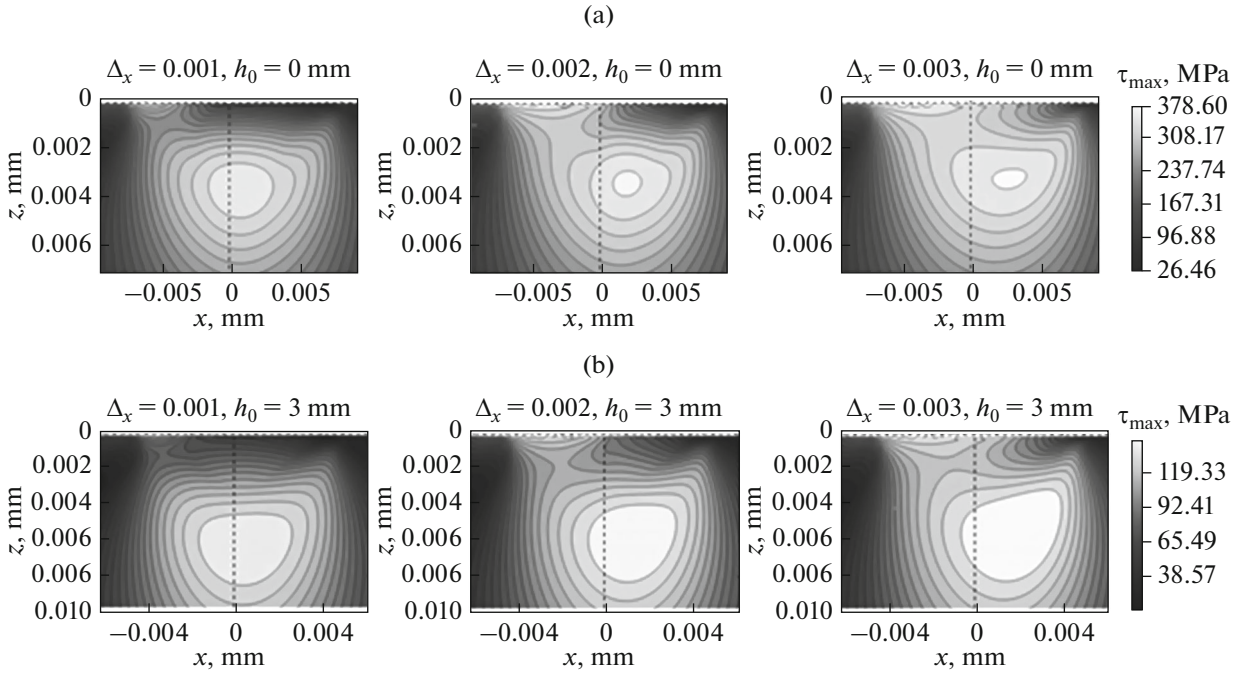

Fig. 6. Dependence of the maximal tangential stresses on the distance to the surface without rail irregularity (a) and at rail irregularity depth $h_0 = 3$ mm (b).

rolling along a rail in a straight section and in the irregularity center are shown in Fig. 6.

According to Figs. 5 and 6, there are two maxima of the function of maximal tangential stresses observed during wheel rolling along the rail. These maxima are surface and subsurface. With an increase in the irregularity depth, both maxima decrease in which case the depth-wise distribution of maximal tangential stresses with irregularity is more even than without irregularity.

At cyclic loads in the wheel-rail system the material of the rail near the rail surface has some initial damage due to the cold-hardening of the surface in the saddling region [15]. Considering a more even depth-wise distribution of maximal tangential stresses, contact-fatigue cracking is more likely near the surface than at depth.

CONCLUSIONS

The wheel–rail interaction during rolling along a straight railroad track section has been modeled with and without the rail flattening. The saddling is used for describing a defect generated in the welded rail joint region. The contact characteristics and stress state of the rail are compared for various relative longitudinal

slip and with and without track irregularities of various depths.

It was found that, with an increase in relative longitudinal slip, the maximum tangential stress on the surface increases. At greater relative slip, the maximum tangential stress function on the surface becomes larger than the subsurface stress, which affects the accumulation of fatigue damage.

The results of analyzing contact pressures and tangential stresses show that, with an increase in the irregularity depth, the maximum contact pressure and tangential stress decrease, and the depth-wise distribution of maximal tangential stresses becomes more uniform. Thus, the considered dimensions of track defects in the region of welded joints in the typical load-speed mode of rolling stock do not lead to an increase in the concentration of subsurface stresses under the wheel–rail contact area in impactless interaction mode.

NOTATION

L	is the longitudinal saddling length
h_0	is the saddling depth
E	is Young's modulus
ν	is Poisson's ratio
a_1, b_1	are the semiaxes of the elliptical contact region
p_{0_1}	is the maximum contact pressure in case of an elliptical contact area
P	is for the full normal wheel load
R_1, R_1'	are the main curvature radii of the wheel
R_2, R_2'	are the main curvature radii of the rail
ψ	is the angle between the normal planes containing curvature radii R_1, R_2
ω, V	are the angular and linear rolling speed of the wheel
t	is time
c	is the stiffness of the spring equivalent to the wheel–rail system
m	is the mass of the unsprung parts
δ	is the static deflection of the wheels
$z_{\max}$	is the additional deformation of the equivalent spring
η	is the load dynamic factor
P_{add}	is the additional dynamic vertical load on the wheel
a_2	is the half-width of the contact area in the direction of the x-axis during the rolling over the rail irregularity
b_2	is half-width of the contact area in the direction perpendicular to the rolling direction
p_{0_2}	is the maximum contact pressure at the rolling over the rail irregularity
R_c	is the curvature radius of the rail irregularity surface in its center
$s(x, y)$	is the longitudinal slip velocity
$u_{1,2}(x, y)$	are the tangential displacements of the wheel and rail
Δ_x	is the relative longitudinal slip
$\tau_{\max}(x, y, z)$	are the maximum tangent stresses
$\sigma_i(x, y, z)$, $i = 1, 2, 3$	are the principal stresses

FUNDING

The study was funded by the Russian Foundation for Basic Research, Sirius University of Science and Technology, JSC Russian Railways, and Educational Fund Talent and Success, project no. 20-38-51005.

REFERENCES

1. Goryacheva, I.G., Torskaya, E.V., and Dobychin, M.N., Modeling the conditions for the formation of contact-fatigue damage to the tread surface, in *Kontaktno-ustalostnye povrezhdeniya koles gruzovykh vagonov* (Contact-Fatigue Damage to Freight Cars Wheels), Zakharov, S.M., Ed., Moscow: INTEKST, 2004, pp. 58–113.
2. Kossov, V.S., Krasnov, O.G., and Akashev, M.G., The impact of deformation in the zone of welded joints on the force action of the rolling stock on the track, *Vestn. Inst. Zheleznodor. Transp.,* 2020, Vol. 79, no. 1, pp. 9–16.
3. Instructions: Rail Defects. Classification, catalog and parameters of defective and sharply defective rails, Approved October 23, 2014.
4. Mikheev, G.V., Pogorelov, D.Yu., and Rodikov, A.N., Methods for wheelset dynamics modeling taking into account elasticity, *Vestn. Bryan. Tekh. Univ.,* 2019, no. 4 (77), pp. 40–51.
5. Xu, J. et al., Geometry evolution of rail weld irregularity and the effect on wheel-rail dynamic interaction in heavy haul railways, *Eng. Fail. Anal.,* 2017, vol. 81, pp. 31–44.
6. Bezgin, N.Ö., Development of a new and an explicit analytical equation that estimates the vertical dynamic impact loads of a moving train, *Proc. Eng.,* 2017, vol. 189, pp. 2–10.
7. Kalker, J.J., A fast algorithm for the simplified theory of rolling contact, *Veh. Syst. Dyn.,* 1982, vol. 11, no. 1, pp. 1–13.
8. Goldstein, R.V. et al., Solutions of three-dimensional rolling problems with slip and adhesion by variational methods, *Usp. Mekh.,* 1982, vol. 5, nos. 3–4, pp. 60–102.

9. Meshcheryakova, A.R. and Goryacheva, I.G., Stress state of elastic bodies with an intermediate layer in rolling contact with slip, *Phys. Mesomech.,* 2021, vol. 24, pp. 441–450.

10. Zakharov, S.M. and Torskaya, E.V., Approaches to modeling occurrence of rolling contact fatigue damages in rails, *Vestn. Inst. Zheleznodor. Transp.,* 2018, vol. 77, no. 5, pp. 259–268.

11. Ekberg, A., Kabo, E., and Andersson, H., An engineering model for prediction of rolling contact fatigue of railway wheels, *Fatigue Fract. Eng. Mater. Struct.,* 2002, no. 10, pp. 899–909.

12. Johnson, K.L., *Contact Mechanics,* Cambridge: Cambridge Univ. Press, 1985.

13. Vershinskij, S.V., Danilov, V.N., and Husidov, V.D., *Dinamika vagona* (Wagon Dynamics), Moscow: *Transport*, 1991.

14. Rabotnov, Yu.N., *Soprotivlenie materialov* (Strength of Materials), Moscow: Fizmatgiz, 1962.

15. Daves, W. et al., A finite element model to simulate the physical mechanisms of wear and crack initiation in wheel/rail contact, *Wear,* 2016, vols. 366–367, pp. 78–83.

Translated by S. Kuznetsov